

## MIT Open Access Articles

*Dense All#Electrochem#Active Electrodes  
for All#Solid#State Lithium Batteries*

The MIT Faculty has made this article openly available. **Please share** how this access benefits you. Your story matters.

**Citation:** Li, M., Liu, T., Shi, Z., Xue, W., Hu, Y.-s., Li, H., Huang, X., Li, J., Suo, L., Chen, L., Dense All-Electrochem-Active Electrodes for All-Solid-State Lithium Batteries. *Adv. Mater.* 2021, 33, 2008723

**As Published:** <http://dx.doi.org/10.1002/adma.202008723>

**Publisher:** Wiley

**Persistent URL:** <https://hdl.handle.net/1721.1/140282>

**Version:** Author's final manuscript: final author's manuscript post peer review, without publisher's formatting or copy editing

**Terms of use:** Creative Commons Attribution-Noncommercial-Share Alike



## Dense All-Electrochem-Active Electrodes for All-Solid-State Lithium Batteries

Meiyong Li<sup>1,2</sup>, Tao Liu<sup>1</sup>, Zhe Shi<sup>3</sup>, Weijiang Xue<sup>3</sup>, Yong-sheng Hu<sup>1</sup>, Hong Li<sup>1</sup>, Xuejie Huang<sup>1</sup>, Ju Li<sup>3\*</sup>, Liumin Suo<sup>1,2,4\*</sup>, Liqun Chen<sup>1</sup>

Meiyong Li, Dr. Tao Liu, Dr. Zhe Shi, Dr. Weijiang Xue, Prof. Yong-sheng Hu, Prof. Hong Li, Prof. Xuejie Huang, Prof. Ju Li, Prof. Liumin Suo, Prof. Liqun Chen

<sup>1</sup>Beijing Advanced Innovation Center for Materials Genome Engineering, Key Laboratory for Renewable Energy, Beijing Key Laboratory for New Energy Material and Devices, Beijing National Laboratory for Condensed Matter Physics, Institute of Physics, Chinese Academy of Science, Beijing 100190, China

<sup>2</sup>Center of Materials Science and Optoelectronics Engineering, University of Chinese Academy of Sciences, Beijing 100049, China

<sup>3</sup>Department of Nuclear Science and Engineering and Department of Materials Science and Engineering, Massachusetts Institute of Technology, Cambridge, MA, USA

<sup>4</sup>Yangtze River Delta Physics Research Center Co. Ltd, Liyang, 213300, China

E-mail: [liju@mit.edu](mailto:liju@mit.edu), [suoliumin@iphy.ac.cn](mailto:suoliumin@iphy.ac.cn)

Keywords: All-electrochem-active electrodes, all-solid-state batteries, energy density, conductive networks

This is the author manuscript accepted for publication and has undergone full peer review but has not been through the copyediting, typesetting, pagination and proofreading process, which may lead to differences between this version and the [Version of Record](#). Please cite this article as [doi: 10.1002/adma.202008723](https://doi.org/10.1002/adma.202008723).

This article is protected by copyright. All rights reserved.

The energy density presents the core competitiveness of lithium (Li)-ion batteries. In conventional Li-ion batteries, the utilization of the gravimetric/volumetric energy density at the electrode level is unsatisfactory (<84wt.% and <62vol.%, respectively) due to the existence of non-electrochemical active parts among the three-dimensional porous electrodes, including electrolytes, binders, and carbon additives. These are regarded as indispensable and irreducible components of the electronic and ionic transport network. Here, we propose a dense all-electrochem-active (AEA) electrode for all-solid-state Li batteries, which is entirely constructed from a family of superior mixed electronic-ionic conducting cathodes, to minimize the energy density gap between the accessible and theoretical energy density at the electrode level. Furthermore, with the ionic-electronic conductive network self-supported from the AEA cathode, the dense hybrid sulfur-based AEA electrode exhibits a high compacted filling rate of 91.8%, which indicates a high energy density of  $777 \text{ W h kg}^{-1}$  and  $1,945 \text{ W h L}^{-1}$  at the electrode level based on the total cathodes and anodes.

## 1. Introduction

The pursuit of high energy density and a safe working process remains a topic of interest in the field of energy storage devices. Following a lengthy competition, lithium (Li)-ion batteries have come to dominate almost all the critical applications, including consumer electronic devices, electric transportation, and electric grid energy storage.<sup>[1, 2]</sup> Compared with the early Li-ion batteries produced by Sony in the 1990s ( $80 \text{ W h kg}^{-1}$ ,  $200 \text{ W h L}^{-1}$  [LiCoO<sub>2</sub>/C]),<sup>[3]</sup> the energy densities of the state-of-the-art Li-ion batteries have increased more than threefold ( $\sim 300 \text{ W h kg}^{-1}$  [NCM811/Si-C],  $\sim 700 \text{ W h L}^{-1}$  [LiCoO<sub>2</sub>/C]).<sup>[4, 5]</sup> However, it is alarming that the energy density of the current type Li-ion batteries is very close to the limit.<sup>[6]</sup> The energy density at the electrode level is not only determined by the theoretical energy density of the electrochemical couples (energy density = average voltage  $\times$  specific capacity) but is also highly sensitive to the weight fraction of the inactive components.<sup>[7, 8]</sup> In addition, the binder and any conductive additives, especially the filling electrolyte, not only limit the

energy density but also involve various security issues. As such, a number of research studies and technologies have been aimed at reducing the fraction of the inactive mass or volume; however, the attendant strategy is, at best, borderline.

In fact, only one case overcomes this barrier, that is, the Li metal anode. The absence of inactive additives and the high energy density ( $\text{Li}^0 \rightarrow \text{Li}^+ + \text{e}^-$ , 3,860 mAh g<sup>-1</sup>, 2,061 mAh L<sup>-1</sup>) ensure it is a prominent representative electrode.<sup>[9,10]</sup> In fact, the Li metal anode can be regarded as an all-electrochem-active (AEA) anode. However, on the cathode side, the realization of an AEA is primarily limited by its insufficient electronic conductivity ( $10^{-4}$ – $10^{-10}$  S cm<sup>-1</sup>), which is over five orders of magnitude lower than the conductive carbon black ( $\sim 10$  S cm<sup>-1</sup>),<sup>[11,12]</sup> and its sluggish Li-ion diffusion coefficient ( $D_{\text{Li}}$ ) ( $10^{-10}$ – $10^{-15}$  cm<sup>2</sup> s<sup>-1</sup>) that is much smaller than the liquid 1M LiPF<sub>6</sub> in dimethyl carbonate–ethylene carbonate electrolytes ( $\sim 2 \times 10^{-6}$  cm<sup>2</sup> s<sup>-1</sup>).<sup>[13, 14]</sup> To guarantee a well interconnected electronic–ionic network, the porous 3D electrode structure of the traditional Li-ion cathode must be uniformly filled with the conductive additive (carbon black), the polymer binder, and the liquid electrolytes, the total weight and volume fractions of which are >10wt.% and >30vol.%, respectively<sup>[15-17]</sup> (Figure 1, see the detailed information in Supplementary Tables S1 and S2).

The equivalent specific capacity ( $ESC = C/m_{\text{electrode}}$ ,  $C$ : the capacity of the cathode,  $m_{\text{electrode}} = m_{\text{cathode}} + m_{\text{binder}} + m_{\text{electrolyte in the electrode}} + m_{\text{conductive additive}}$ ) is defined to assess the capacity of the electrode, accounting for the overall impacts of the active cathode and the non-active parts, including the binder, carbon black, and electrolyte filling in the electrode. Based on the  $ESC$ , we can obtain the energy density of the electrode ( $EG_{\text{electrode}} = ESC \times V$ ,  $V$ : discharge voltage). This indicates that the above compromises dilute the electrode-level energy density by at least 16%. Compared with the liquid-electrolyte-based electrode, the solid-state electrolyte (SSE)-based electrodes perform better in terms of security; however, perhaps unsurprisingly, they exhibit a lower  $ESC_{\text{electrode}}$  due to their higher densities (oxide-based electrolyte: 2.93~5.07 g cm<sup>-3</sup>, sulfide-based electrolytes: 1.87~1.97 g cm<sup>-3</sup>, PEO-based: 1.2~1.25 g cm<sup>-3</sup>) and far more SSEs are required to ensure physical contact.<sup>[18,19]</sup> According to the existing data,<sup>[20-22]</sup> the weight fraction of cathode materials in all-solid-state Li batteries (ASSLBs) is less than 80wt.% (Figure 1d and e, see the detailed information

in Supplementary Tables. S1~S3), which results in low  $ESC_{electrode}$  ( $0.8 \times$  specific capacity) for this type of battery. In ASSLBs, it is theoretically possible to achieve an AEA electrode if the Li-containing cathode has high enough ionic and electronic conductivity, where the electrode is 100% occupied by active cathode materials and the Li-ion and electron transportation is self-actuating (Figure 1c).

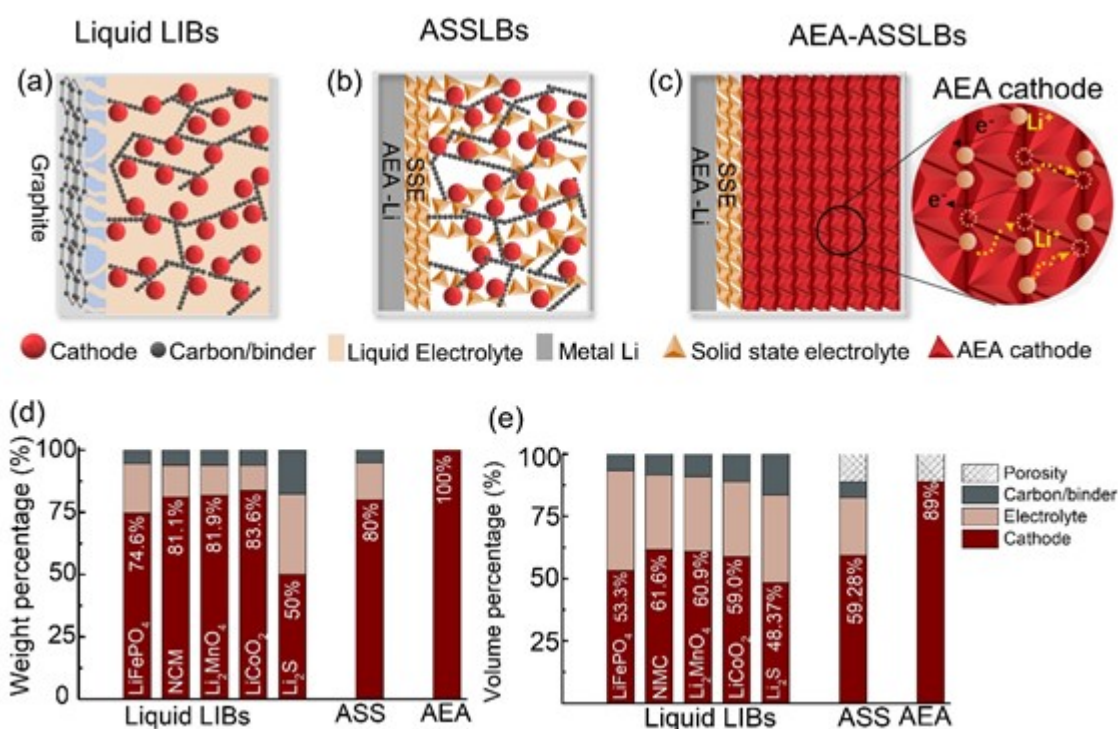


**Figure 1.** The concept of all-electrochem-active electrodes: a). Commercial liquid Li-ion batteries (74.6~83.6wt% Cathode, Anode: Graphite); b). conventional ASSLBs (80wt% Cathode, Anode: Li metal); c). our proposed AEA-ASSLBs (100wt% AEA Cathode, Anode: Li metal), d) and e). summaries of the weight and volume percentages of various components.

### The concept of all-electrochem-active electrodes

In conventional Li-ion cathodes, the Li-ions reach the cathode through the electrolyte and electrons from the external circuit to the cathode and react at the three-phase interface (carbon/electrolyte/electroactive mass).<sup>[23, 24]</sup> However, it is significant that the Li-ion and electron

transportation self-relies on the all-in-one active electrode in our proposed AEA electrodes, the weight and volume percentages of which can increase to 100% and 89% (porosity 11 %), respectively, in the electrode. To realize our idea, the ideal AEA candidates should have fast Li-ion transportability (alternative to electrolyte), high electronic conductivity (alternative to the conductive additive), and abundant lithium storage sites (electrochemical active capacity). Furthermore, the ideal candidate would have a stable fixing structure with a low fluctuation of ionic and electronic conductivity that varies according to Li-ion concentration.

Following careful screening, a series of conductive transition metal sulfides caught our attention.<sup>[25-28]</sup> In previous works, pure amorphous transition metal sulfide cathodes were used as the electrode in all-solid-state batteries.<sup>[29-31]</sup> However, their electronic conductivity ( $\sim 10^{-3}$  S cm<sup>-1</sup>) is four orders of magnitude lower than carbon ( $\sim 10$  S cm<sup>-1</sup>),<sup>[32]</sup> and their ionic conductivity is not particularly stable during the charge-discharge process. In our work, we selected crystal transition metal sulfides, namely, layer-structured TiS<sub>2</sub> and chevreil-phase Mo<sub>6</sub>S<sub>8</sub>, which not only have a very stable host structure but also high electronic conductivity.<sup>[33]</sup> Mo<sub>6</sub>S<sub>8</sub> and TiS<sub>2</sub> have a high electronic conductivity, which is over 3-6 orders of magnitude higher than that of the typical cathode materials (NMC532 and carbon-coated LiFePO<sub>4</sub>), and comparable to the commercial conductive carbon (Super P) (Figure 2a, see the detailed information in Supplementary Table S4). These super-high electronically conducting TiS<sub>2</sub> and Mo<sub>6</sub>S<sub>8</sub> materials allow for eliminating the conductive carbon in the electrode. In addition, Mo<sub>6</sub>S<sub>8</sub> and TiS<sub>2</sub> have a high Li-ion diffusion coefficient of  $1.8\sim 9.8 \times 10^{-8}$  cm<sup>2</sup> s<sup>-1</sup> and  $8 \times 10^{-9}\sim 9 \times 10^{-10}$  cm<sup>2</sup> s<sup>-1</sup> (see the detailed information in Supplementary Figure S1),<sup>[25, 34, 35]</sup> which is comparable to that of SSEs (Li<sub>10</sub>GeP<sub>2</sub>S<sub>12</sub>,  $8.8\sim 9 \times 10^{-8}$  cm<sup>2</sup> s<sup>-1</sup>, Li<sub>10</sub>SiP<sub>2</sub>S<sub>12</sub>,  $7\sim 7.2 \times 10^{-8}$  cm<sup>2</sup> s<sup>-1</sup>, Li<sub>6.25</sub>Al<sub>0.25</sub>La<sub>3</sub>Zr<sub>2</sub>O<sub>12</sub>,  $1\sim 1.1 \times 10^{-8}$  cm<sup>2</sup> s<sup>-1</sup>) and far higher than that of the conventional commercial cathodes (LiFePO<sub>4</sub>:  $6.8 \times 10^{-16}\sim 1.8 \times 10^{-14}$  cm<sup>2</sup> s<sup>-1</sup>, NMC:  $2.8\sim 8 \times 10^{-11}$  cm<sup>2</sup> s<sup>-1</sup>, LiCoO<sub>2</sub>:  $10^{-11}\sim 10^{-12}$  cm<sup>2</sup> s<sup>-1</sup>) (Figure 2b, see the detailed information in Supplementary Table S5).<sup>[36-45]</sup> As such, they can serve as solid electrolytes rather than filling electrolytes in the electrodes. Meanwhile, the intercalation compounds of Mo<sub>6</sub>S<sub>8</sub> and TiS<sub>2</sub> enable Li-ion storage in their host with the high stability of the host framework structure and the low fluctuation of ionic and electronic conductivity. Based on the above merits of the physicochemical properties, we decided to use full electrochemical active electrodes (100% Mo<sub>6</sub>S<sub>8</sub> or TiS<sub>2</sub> cathode and Li metal anode) to construct an ASSLB.

### Demonstration of all-electrochem-active all-solid-state lithium batteries

To provide a proof-of-concept, AEA–ASSLBs were constructed using a configuration of AEA cathode (100%  $\text{TiS}_2$  or  $\text{Mo}_6\text{S}_8$ )/SSEs ( $\text{Li}_{10}\text{GeP}_2\text{S}_{12}$ - $\text{L}_3\text{PS}_4$ )/AEA anode (100% Li metal anode).<sup>[46]</sup> As shown in Figure 2c and Figure 2d, the  $\text{TiS}_2$ -based AEA–ASSLBs had an initial discharge capacity of 213  $\text{mAh g}^{-1}$  at 70°C with the characteristic smooth slope in the voltage profile demonstrating the solid-solution reaction. Meanwhile, the  $\text{Mo}_6\text{S}_8$ -based AEA–ASSLBs delivered a capacity of 130  $\text{mAh g}^{-1}$ , with two characteristic well-defined plateaus in the voltage profile corresponding with the two-phase reaction (2.3V,  $\text{Mo}_6\text{S}_8 \rightarrow \text{LiMo}_6\text{S}_8$ , and 2.05 V,  $\text{LiMo}_6\text{S}_8 \rightarrow \text{Li}_3\text{Mo}_6\text{S}_8/\text{Li}_4\text{Mo}_6\text{S}_8$ ) (Figure 2d). Since both pristine  $\text{TiS}_2$  and  $\text{Mo}_6\text{S}_8$  are lithium-free, a partial pre-lithiation was required to provide the function of a Li-ion conductor on the initial discharge. Specifically, the observed capacity gap between the first and second discharge roughly correlates with the lithium consumption of the pre-lithiation process corresponding with  $\text{Li}_{0.1}\text{TiS}_2$  (LTS) (25  $\text{mAh g}^{-1}$ ) and  $\text{LiMo}_6\text{S}_8$  (LMS) (35  $\text{mAh g}^{-1}$ ). Starting with these very partially pre-lithiated materials (LTS and LMS), the batteries had a reversible capacity of more than 180  $\text{mAh g}^{-1}$  for LTS and 90  $\text{mAh g}^{-1}$  for LMS, demonstrating that our AEA–ASSLBs can work well based on both solid-solution (LTS) and two-phase reaction (LMS) mechanisms. In sharp contrast, the AEA electrode constructed using the typical  $\text{LiFePO}_4$  and  $\text{Li}_4\text{T}_5\text{O}_{12}$  materials failed (see the detailed information in Supplementary Figure S2). Compared with the LTS, the LMS exhibited better cycling stability with a high capacity retention of 89% after 50 cycles (compared with the 2nd cycle).

Author Manuscript

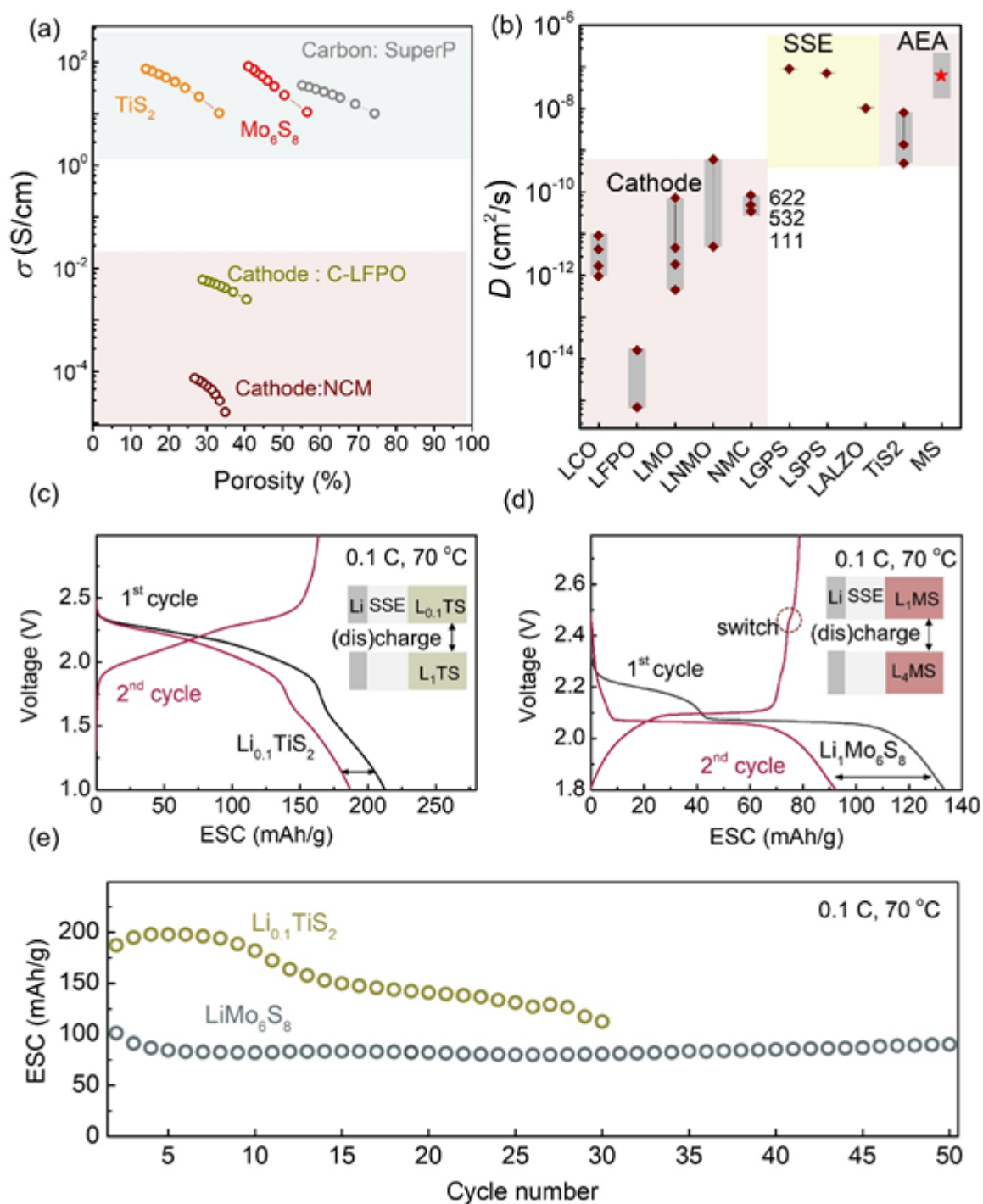


**Figure 2. The proof-of-concept of the AEA-ASSLBs:** a). Electronic conductivities of our AEA materials in comparison with the available conductive carbon additives and traditional cathodes, obtained via the 4-electrode powder electronic conductivity test, b). Li-ion diffusion coefficients of our AEA

This article is protected by copyright. All rights reserved.



materials obtained via the potentiostatic intermittent titration technique method in comparison with the available traditional cathodes and typical SSEs, c) and d). the galvanostatic discharge–charge profiles of the  $\text{Li}_{0.1}\text{TiS}_2$ - and  $\text{LiMo}_6\text{S}_8$ -based AEA cathodes, e). their corresponding cycling stabilities at 0.1C/70°C.

The aforementioned distinctions could be attributed to the materials' intrinsic physicochemical properties, crystal structure, and different Li storage mechanisms. LTS presents a solid-solution reaction involving Li-vacancy disorder, the Li-ion diffusion coefficient of which largely depends on the vacancy concentration and is susceptible to the Li concentration.<sup>[47]</sup> Upon cycling, any trapping Li for the irreversible capacity loss could potentially gradually lower the kinetic of the LTS–AEA electrode, resulting in capacity fade (Figure 2e). In contrast, LMS maintains a high  $D_{\text{Li}}$  with a very low fluctuation from  $1.8 \times 10^{-8}$  to  $1.7 \times 10^{-7} \text{ cm}^2 \text{ s}^{-1}$  (Figure 3a). The C-rate performance also verified the fast kinetic of Li-ion transportation, and the LMS–AEA electrode with a high cathode mass loading of  $13.91 \text{ mg cm}^{-2}$  (compacting density is  $4.5 \text{ g cm}^{-3}$  and the thickness of electrode is  $30.9 \text{ }\mu\text{m}$ ) eliminates the possibility that the capacity only originates from the interfacial electrochemical reaction between the LMS and the SSE (see the detailed information in Supplementary Figures S3 and S4). Furthermore, our LMS–AEA electrode exhibited superior plasticity, which enabled elastic recovery after releasing the pressure. As the apparent gap in porosity marked by the shadowed area in Figure 3b indicates, the porosity of  $\text{Mo}_6\text{S}_8$  decreased to 11% under 360 MPa (the applied pressure of ASSLBs in real operating conditions) and rebounded to 24% after the pressure was released (see the detailed information in Supplementary Tables S6 and S7). The excellent deformability of the LMS–AEA electrode is not only favorable in terms of achieving a dense electrode and good physical solid–solid interfacial contact but is also helpful for buffering the volume expansion of cathode materials during cycling. Thus, in the following section, LMS is selected as our priority material.

To verify the phase transformation during charging, *in-situ* X-ray diffraction (XRD) was performed for a tailor-made all-solid-state battery (Figure 3c). The pristine electrode belongs to the  $\text{Li}_0$  phase ( $\text{Mo}_6\text{S}_8$ ) [JCPDC: 89-5114] with three major peaks at  $30.7^\circ (12\bar{1})$ ,  $33.9^\circ (21\bar{2})$ , and  $34.8^\circ (104)$ . At the initial stage of the discharge, a new  $\text{Li}_1$  phase ( $\text{LiMo}_6\text{S}_8$ ) [JCPDC: 81-0858,  $30.4^\circ (12\bar{1})$ ,  $33.7^\circ (21\bar{2})$ , and  $35.0^\circ (104)$ ] was generated along with a decrease in the intensity of the  $\text{Li}_0$ ,

indicating the two-phase transformation between  $\text{Li}_0$  and  $\text{Li}_1$ . Subsequently, along with a second discharge plateau (2.05 V), the  $\text{Li}_1$  phase further transformed into a  $\text{Li}_3$  phase [JCPDS81-0859,  $32.7^\circ$  ( $21\bar{2}$ ),  $35.5^\circ$ (104) and  $36.8^\circ$ (220)] and finally converted into  $\text{Li}_4\text{Mo}_6\text{S}_8$  ( $\text{L}_4$  phase) [JCPDS: 81-0860,  $32.6^\circ$  ( $21\bar{2}$ ),  $35.4^\circ$  (104) and  $36.7^\circ$  (220)]. To further quantify the relative content of the different phases in the two-phase coexistence region, the normalized intensity based on the ( $21\bar{2}$ ) peak was obtained, as shown in Figure 3d (middle). This revealed clear multiple two-phase coexistences that were consistent with the charge–discharge profiles (Figure 2d). The final discharge product of  $\text{Li}_4$  can only be reversibly converted into  $\text{Li}_1$  with a trace of  $\text{L}_0$  phase remaining that corresponds with the very short plateau at 2.45 V at the end of the charge stage (circled in Figure 3c, right). The LMS–AEA electrode processes a step-wise electrochemical reaction with the multiple phase transformations in the first cycle, which can be divided into four stages in the order of stage I, stage II, stage III, and stage IV (Figure 3c, middle). During stage I and II, the increase in Li concentration promotes Li-ion transportation in the AEA electrode due to the formation of  $\text{Li}_x\text{Mo}_6\text{S}_8$  ( $x = 1, 3, 4$ ) with a high diffusion coefficient  $D_{\text{Li}}$ . The high Li concentration phases gradually transformed into low phases during de-lithiation (stage III) ( $\text{Li}_4$ - $\text{Li}_3$ - $\text{Li}_1$ ). At the end of stage IV, an ionically blocking interphase layer mainly consisting of  $\text{Li}_0$  formed since this is a lithium-free and ionic-isolating phase, and its formation on the interface of the electrode–electrolyte shut down the further phase transformation from  $\text{Li}_1$  to  $\text{Li}_0$  in the bulk electrode, much like a specific “ionic switch.” At this time, the de-lithiation process is blocked and  $\text{Li}_1$  is retained to a large extent. These results confirmed our hypothesis that the LMS–AEA electrode requires an initial partial pre-lithiation such that its Li ionic and electronic conductivities are qualified.

Author

This article is protected by copyright. All rights reserved.

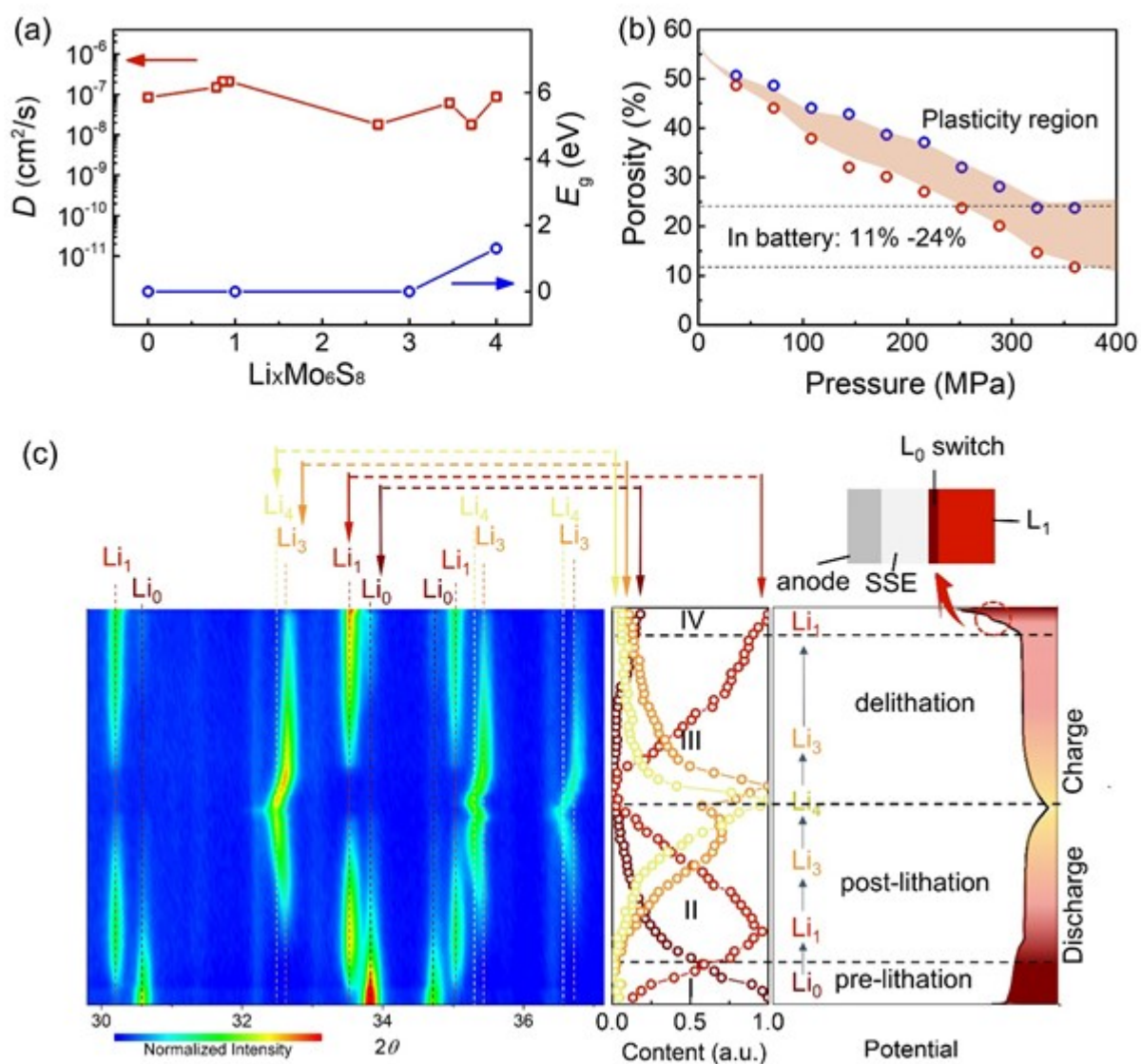
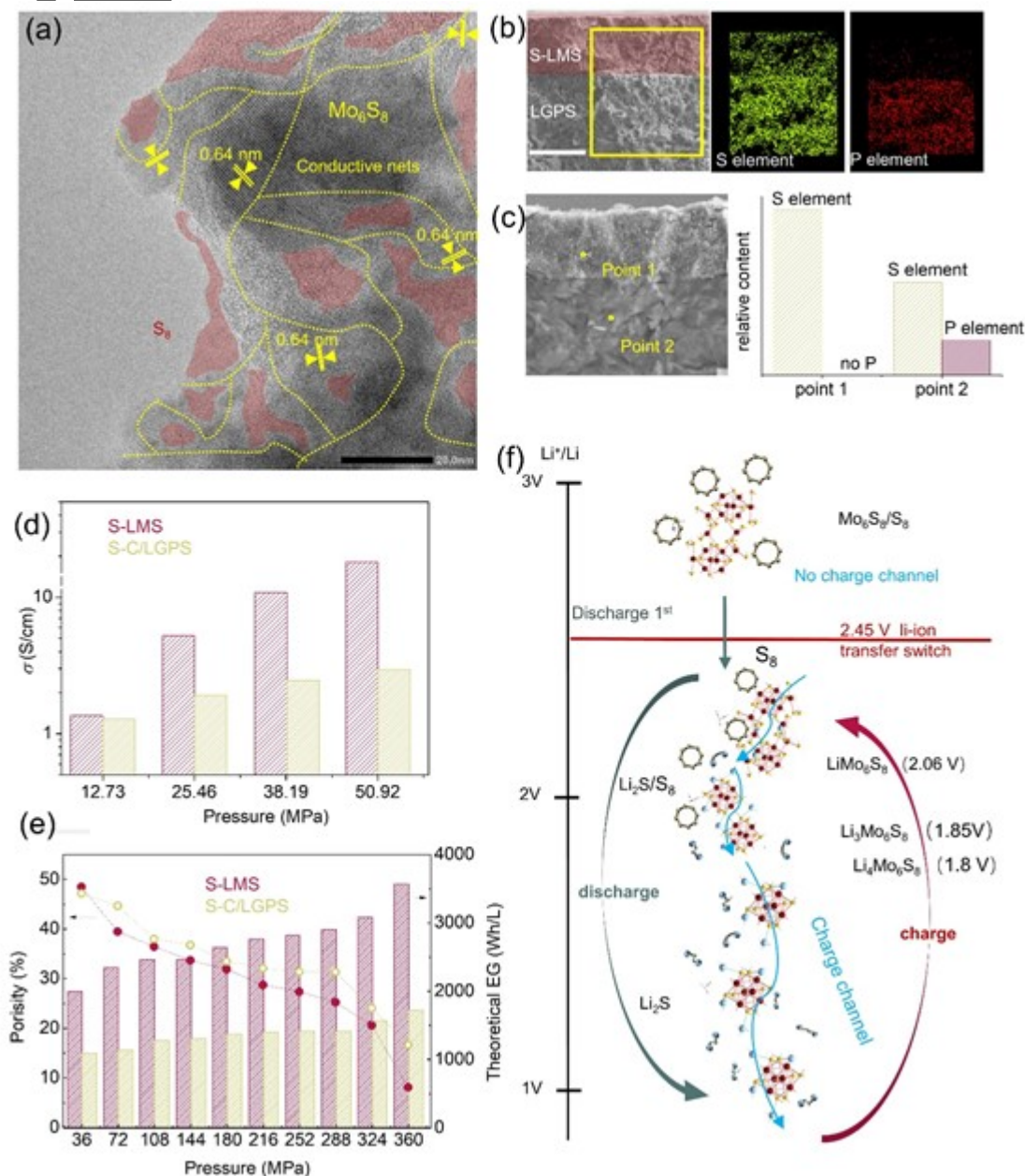


**Figure 3. The electrochemical mechanism of the LMS-based AEA cathode:** a). Li-ion diffusion coefficients and energy bandgap of  $\text{Li}_x\text{Mo}_6\text{S}_8$  ( $x = 0, 1, 3, 4$ ), b). the porosity of the AEA  $\text{Mo}_6\text{S}_8$  electrode as a function of the applied pressure. The red circles represent the value test with pressure, and the blue ones represents the value test releasing the pressure, c). In-situ XRD analysis of the LMS-based AEA cathode (left). The normalized intensity of the peak at  $33.9^\circ$  ( $\text{Li}_0$ ),  $33.7^\circ$  ( $\text{Li}_1$ ), and  $32.7^\circ$  ( $\text{Li}_{3-4}$ ) in different stages (middle) and the phase transition process accompanying the charge–discharge profiles (right).

Based on the above results and discussion, we have successfully demonstrated the proof-of-concept of the AEA electrode in ASSLBs. This AEA electrode can also work at room temperature (see the detailed information in Supplementary Figures. S5). However, compared with conventional Li-ion batteries, the  $ESC_{electrode}$  of the LMS–AEA cathode was only  $90 \text{ mA h g}^{-1}$ , which means that it had not yet realized its full potential in terms of energy density. To further display the advantages of the AEA electrode, a hybrid sulfur– $\text{Mo}_6\text{S}_8$  (S-LMS)-based AEA cathode was attempted, since an S cathode has a high theoretical capacity of  $1,675 \text{ mA h g}^{-1}$ , with redox potentials ideally below the “ionic switch” of 2.45 V.<sup>[48-51]</sup> Given that a  $\text{S}_8$  cathode is electronically insulating, the conductive LMS served as an efficient electronically and ionically conducting network within the AEA electrode, with the weight percentages of  $\text{S}_8$  and  $\text{Mo}_6\text{S}_8$  32.5wt% and 67.5wt%, respectively. The transmission electron microscopy (TEM) image of the hybrid S-LMS–AEA cathode (Figure 4a) revealed the coexistence of amorphous  $\text{S}_8$  (marked by the yellow-block) and crystalline  $\text{Mo}_6\text{S}_8$  (marked by the green lines), the electron diffraction patterns are shown in Figure S6 and the XRD patterns are shown in S7. Inside the electrode, the small  $\text{Mo}_6\text{S}_8$  nano-sheets were mutually interconnected and thus constructed a conductive network for electrons/ions transport. Furthermore, the amorphous  $\text{S}_8$  was homogeneously dispersed, which was reflected by the 10–30 nm nano-domain distributed in the  $\text{Mo}_6\text{S}_8$  framework that guarantees the desired electrons/ions transport in the insulating  $\text{S}_8$ . Unlike conventional all-solid-state Li-S cathodes with three single-function materials (carbon/SSE/S) for forming three-phase reaction interfaces, our hybrid S-LMS–AEA cathode had an all-in-one ionically/electronically transporting two-phase reaction interface (LMS/S), which allows for avoiding the unbalanced transport between the electron (by carbon) and Li-ion (by the SSEs).

Figure 4b shows the cross-sectional images and the elemental mapping of the hybrid S-LMS–AEA cathode and the  $\text{Li}_{10}\text{GeP}_2\text{S}_{12}$  SSE. The local element distribution of the phosphorus (P) indicated a pure AEA cathode electrode without any SSE component (see the detailed information in Supplementary Figures S8 ~ S10), which was confirmed by the obtained energy-dispersive spectrum, as shown in Figure 4c. Furthermore, the volumetric density at the electrode level is highly dependent on the porosity, which can be reduced by applying pressure in ASSLBs. It is significant that our S-LMS–AEA electrode had a very high compacted filling rate of 91.8% at 360 MPa, which was due to the creep of the soft  $\text{Mo}_6\text{S}_8$  and  $\text{S}_8$  (Figure 3b and Figure 4d, see the detailed information in

Supplementary Tables S6 and S8), the 8.2% residual porosity of which allowed for accommodating the volume expansion. Combining the advantages of AEA electrodes in terms of ESC, the theoretical volumetric density of the S-LMS–AEA electrode was estimated to be above 3,565.3 Wh L<sup>-1</sup> (in terms of the volume of the Mo<sub>6</sub>S<sub>8</sub> and S<sub>8</sub>), which is more than double that of the conventional S-C-LGPs (32.5wt%, 17.5wt%, 50wt%) electrode with the same fraction of sulfur.



A

This article is protected by copyright. All rights reserved.

**Figure 4. The structure and electrochemical mechanism of the hybrid S-LMS–AEA cathode (32.5%S<sub>8</sub>–67.5%Mo<sub>6</sub>S<sub>8</sub>).** a). TEM image of the S-LMS–AEA cathode, b). the cross-sectional SEM images of the AEA cathode/Li<sub>10</sub>GeP<sub>2</sub>S<sub>12</sub> interface with the energy dispersive spectrometer (EDS) mapping of the P and S elements, c). EDS point analysis of the P and S elements in the AEA cathode (Point 1) and the Li<sub>10</sub>GeP<sub>2</sub>S<sub>12</sub> (Point 2). The black scale in a is 20 nm, and the white scales in b) and c) are 50 μm. d) and e). Comparison of the electronic conductivities, theoretical volumetric energy density, and porosity of the S-LMS–AEA cathode and those of a typical S-C-LGPS cathode (32.5wt%, 17.5wt%, 50wt%, see the detailed information in Supplementary Figure S11), f). the electrochemical redox mechanism of the S-LMS–AEA cathode.

As Figure 4f illustrates, we proposed a possible electrochemical mechanism for a hybrid S-LMS–AEA cathode. Below 2.45V, the AEA Mo<sub>6</sub>S<sub>8</sub> electrode was first pre-lithiated into LMS before it was reversibly transformed into the following Li-rich phases (Li<sub>1</sub> ↔ Li<sub>4</sub>). Moreover, simultaneously, the S<sub>8</sub> cathode underwent a conversion of S ↔ Li<sub>2</sub>S, delivering a specific capacity of 1,290 mA h g<sup>-1</sup> (by the initial electrode mass, before discharge without Li). The ESC electrode was used instead of the specific capacity for the cathode to evaluate the energy density at the electrode level. In terms of the hybrid S-Mo<sub>6</sub>S<sub>8</sub>–AEA cathode with the Li metal, a high ESC electrode of 483 mA h g<sup>-1</sup> (the theoretical value is 630 mA h g<sup>-1</sup>, supplementary material) was achieved after three cycles, with gravimetric and volumetric energy densities of 905.5 W h kg<sup>-1</sup> and 2,778 W h L<sup>-1</sup>, respectively, at the electrode level, which was close to the theoretical energy density of 1,260 W h kg<sup>-1</sup> and 3,865 W h L<sup>-1</sup> (Figure 5a, see the detailed information in the Supplementary calculation model). Meanwhile, in terms of the discharge products, Li<sub>2</sub>S and Li<sub>4</sub>Mo<sub>6</sub>S<sub>8</sub>, the values were 777 W h kg<sup>-1</sup> and 1,945 W h L<sup>-1</sup>, which is still higher than those of the commercial high-density LiCoO<sub>2</sub> electrode (476 W h kg<sup>-1</sup>, 1,698 W h L<sup>-1</sup>, by the electrode mass) (see the detailed information in Supplementary Table S8). Furthermore, to demonstrate the cycling stability of our hybrid S-LMS–AEA cathode, a Li-In AEA anode was applied to stabilize the interface between the Li metal anode and the SSE. This demonstrated that our AEA ASSLBs had excellent cycling stability with a capacity retention of 76% after 120 cycles (compared to the 30th cycle with the highest energy density, Figure 5c and d).

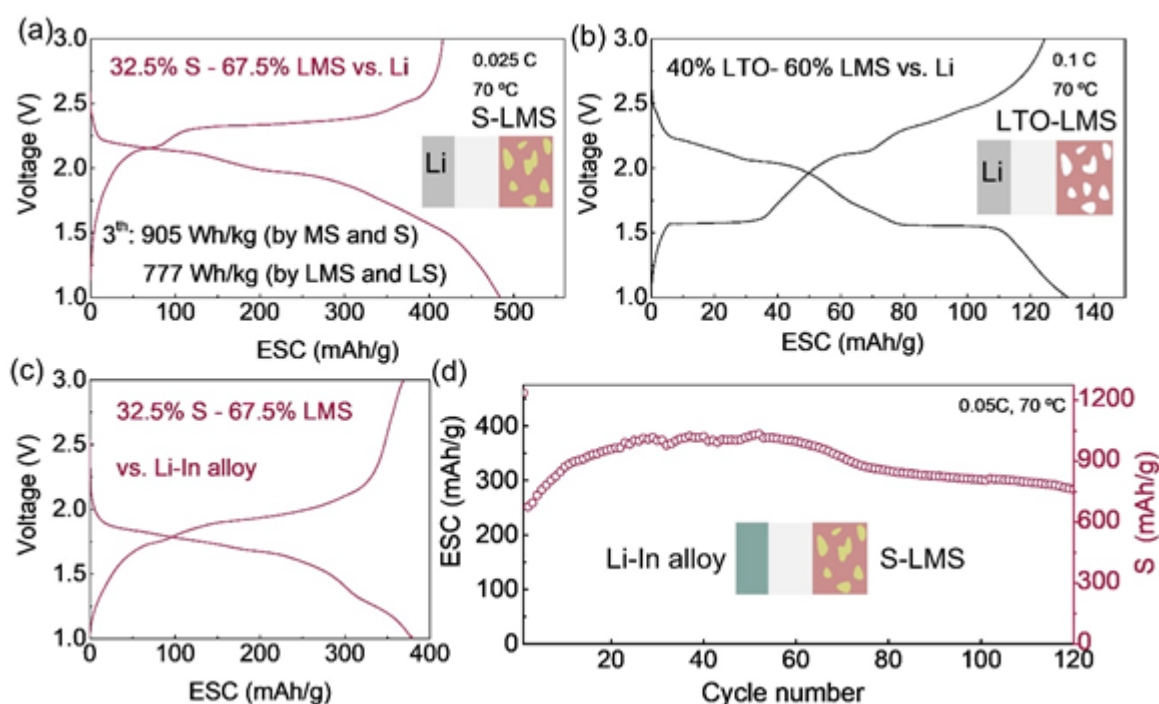


**Figure 5.** The strategies for high energy density AEA-ASSLBs. a)–c). Typical charge–discharge profiles of ASSLBs with hybrid S-LMS (32.5% S<sub>8</sub>-67.5% Mo<sub>6</sub>S<sub>8</sub>) vs. Li, LTO–LMS (40% Li<sub>4</sub>Ti<sub>5</sub>O<sub>12</sub>-60% Mo<sub>6</sub>S<sub>8</sub>) vs. Li, and S-LMS vs. Li-In alloy anode. d). Cycling stabilities of the AEA battery with the S-LMS cathode. The capacity was calculated based on the  $ESC_{electrode}$ .

Our hybrid S-LMS–AEA cathode exhibited the following significant advantages: (1) the electrodes were constructed using 100% electrochemically active substances without any inactive materials, thereby maximizing the cathode capacities at the electrode level. (2) The all-in-one electronic/ionic conductive network of the LMS cathode is favorable in terms of enhancing the electrode kinetic through avoiding the unbalance and inhomogeneous reaction at the three-phase reacting interfaces (carbon/electrolyte/S). (3) Both the AEA cathode and the SSEs belong to the sulfur family, which allows for excellent mutual compatibility through their high affinity. (4) The elastic nature of the AEA cathode alleviates the volume expansion of the S<sub>8</sub>/Li<sub>2</sub>S during cycling. In principle, the LMS–AEA cathode has strong universality, combined with other active materials with a redox potential of less than 2.45V possible. For example, another type of hybrid AEA cathode with

40%  $\text{Li}_4\text{Ti}_5\text{O}_{12}$  and 60%  $\text{Mo}_6\text{S}_8$  (LTO–LMS) exhibited superior cycling stability, with an  $ESC_{\text{electrode}}$  of 130  $\text{mA h g}^{-1}$  at the electrode level (Figure 5b, c, and d).

## Conclusion

We proposed a new concept of all-electrochem-active all-solid-state electrodes with a superior electronic/ionic mixing conductor as an alternative to carbon black and the electrolyte in the electrode. With consideration of our AEA principle and the screening criteria, the LTS- and LMS-based AEA electrodes were selected due to their high electronic conductivity, high ionic diffusion coefficient, and stable Li-storage performance. In these AEA electrodes, the energy density gap at the electrode level between the accessible and the theoretical value is bridged and minimized as far as possible. More significantly, due to the ionically/electronically conductive network self-supported by the AEA cathode material, it can be combined with a high-capacity sulfur cathode to construct a hybrid S-LMS-based AEA cathode with high energy densities of over 770  $\text{W h kg}^{-1}$  and 1,900  $\text{W h L}^{-1}$  at the electrode level. In the future, we believe that AEA electrodes will provide a new means of increasing the energy densities of batteries, regardless of the discovery of new materials. Furthermore, there is the possibility of increasing the energy density by exploring new AEA material candidates with a higher capacity and high voltage that effectively match the 4 V transition metal-oxide cathodes.

## Experimental Section/Methods

*Preparation of AEA cathode:* The  $\text{Mo}_6\text{S}_8$  was synthesized by methods previously reported. The  $\text{TiS}_2$  (99.9%),  $\text{S}_8$  (99.95%, Innochem),  $\text{Li}_4\text{Ti}_5\text{O}_{12}$  (99%),  $\text{Li}_{10}\text{GeP}_2\text{S}_{12}$  (2-5 $\mu\text{m}$ , Kejing star),  $\text{Li}_3\text{PS}_4$  (2-5 $\mu\text{m}$ , Kejing star), Li (99.95%, 80  $\mu\text{m}$ , CEL) and In (99.999%, 30  $\mu\text{m}$ ) foils were obtained commercially. For LMS and LTS-based AEA cathode, the  $\text{Mo}_6\text{S}_8$  and  $\text{TiS}_2$  are using as the AEA electrode without further treatment. For hybrid S-LMS and LTO-LMS based AEA cathode, the  $\text{S}_8/\text{Mo}_6\text{S}_8$  and  $\text{Li}_4\text{Ti}_5\text{O}_{12}/\text{Mo}_6\text{S}_8$  were mixed in 32.5:67.5 by weight (162.5 mg, 337.5 mg,) and 40:60 by weight (200mg, 300mg). Then



put them in an agate mortar for the ball-milling with 300r, 12h, and 300 r, 4 h to prepare the hybrid AEA cathode, respectively.

*Batteries Assembly:* The AEA-ASSLBs batteries are assembled by the configuration of AEA cathode/LGPS/Li<sub>3</sub>PS<sub>4</sub>/Li(In). A mass of 100 mg LGPS and 50mg Li<sub>3</sub>PS<sub>4</sub> solid-state electrolyte (SSE) was uniaxially compressed at about 216 MPa. Then the AEA cathode was added on top of the SSE and distributed homogenously and compressed at 360 MPa. A thickness of 80 μm Li foil was added (accompanying a 30 μm In foil, depending on the experimental designing.) The photography and schematic plot are shown in supplementary material Figure S12.

*Characterization:* The morphologies of the samples were investigated by SEM and TEM. The *in-situ* XRD patterns of the all-solid-state battery were measured using Cu Kα radiation on an X-ray diffractometer from 29.8° to 37.5°(2θ), under 70°C. The electrochemistry was conducted on a LAND battery test station at 70°C. The electronic conductivities of the powder materials were measured by the 4-probe method at room temperature and atmosphere, and the Li-ion diffusion coefficient was measurement by potentiostatic intermittent titration technique. More details of the materials, and characterizations are provided in supplementary material.

### Supporting Information

Supporting Information is available from the Wiley Online Library or from the author.

Received: ((will be filled in by the editorial staff))

Revised: ((will be filled in by the editorial staff))

Published online: ((will be filled in by the editorial staff))

## References

- [1] J. M. Tarascon, M. Armand, *Nature* **2001**, *414*, 359.
- [2] J. B. Goodenough, Y. Kim, *Chem. Mater.* **2010**, *22*, 587.
- [3] T. T. Nagaura, *Prog. Batteries Solar Cells* **1990**, *9*, 209.
- [4] H. Li, *Joule* **2019**, 911.
- [5] X. Wang, Y. L. Ding, Y. P. Deng, Z. Chen, *Adv. Energy Mater.* **2020**, *10*, 1903864
- [6] J. Janek, W. G. Zeier, *Nat. Energy* **2016**, 16141.
- [7] B. J. Landi, M. J. Ganter, C. D. Cress, R. A. DiLeo, R. P. Raffaele, *Energy Environ. Sci.* **2009** *2*, 638.
- [8] H. Zheng, R. Yang, G. Liu, X. Song, V. S. Battaglia, *J. Phys. Chem. C.* **2012**, *116*, 4875.
- [9] W. Xu, J. Wang, F. Ding, X. Chen, E. Nasybulin, Y. Zhang, J. Zhang, *Energy Environ. Sci.* **2014**, *7*, 513.
- [10]. X. Shen, H. Liu, X. B. Cheng, C. Yan, J. Q. Huang, *Energy Storage Mater.* **2018**, *12*, 161.
- [11]. B. Caglar, P. Fischer, P. Kauranen, M. Karttunen, P. Elsner, *J. Power Sources* **2014**, *256*, 88.
- [12]. J. Ni, Y. Li, *Adv. Energy Mater.* **2016**, *6*, 1600278.

This article is protected by copyright. All rights reserved.

- [13]. S. Indris, R. Heinzmann, M. Schulz, A. Hofmann, *J. Electrochem. Soc.* **2014**, *161*, A2036.
- [14]. S. G. Stewart, J. Newman, *J. Electrochem. Soc.* **2008**, *155*, F13.
- [15]. W. Bauer, D. Nötzel, V. Wenzel, H. Nirschl, *J. Power Sources* **2015**, *288*, 359.
- [16]. N. Besnard, A. Etienne, T. Douillard, O. Dubrunfaut, P. T. Van, L. Gautier, S. Franger, J. C. Badot, E. Maire, and B. Lestriez, *Adv. Energy Mater.* **2017**, *7*, 1602239.
- [17]. E. J. Berg, C. Villevieille, D. Streich, S. Trabesinger, P. Novák, *J. Electrochem. Soc.* **2015**, *162*, A2468.
- [18]. S. Skaarup, K. West, B. Z. Christiansen, *Solid State Ionics* **1988**, *28*, 975.
- [19]. L. Liu, J. Xu, S. Wang, F. Wu, H. Li, L. Chen, *eTransportation* **2019**, *1*, 100010.
- [20]. R. Xu, J. Yue, S. Liu, J. Tu, F. Han, P. Liu, *ACS Energy Lett.* **2019**, *4*, 1073.
- [21]. Y.G. Lee, S. Fujiki, C. Jung, N. Suzuki, N. Yashiro, R. Omoda, D. S. Ko, T. Shiratsuchi, T. Sugimoto, S. Ryu, J. H. Ku, T. Watanabe, Y. Park, Y. Aihara, D. I. T. Han, *Nat. Energy* **2020**, *5*, 299.
- [22]. Z. Wan, D. Lei, W. Yang, C. Liu, K. Shi, X. Hao, L. Shen, W. Lv, B. Li, Q. H. Yang, F. Kang, and Y. B. He, *Adv. Funct. Mater.* **2019**, *29*, 1805301.
- [23]. H. Bockholt, M. Indrikova, A. Netz, F. Golks, A. Kwade, *J. Power Sources* **2016**, *325*, 140.
- [24]. Y. H. Chen, C. W. Wang, X. Zhang, A. M. Sastry, *J. Power Sources* **2010**, *195*, 2851.
- [25]. A. J. Vaccaro, T. Palanisamy, R. L. Kerr, J. T. Maloy, *Solid State Ionics* **1981**, *2*, 337.

- [26]. M. Pan, T. Hakari, A. Sakuda, A. Hayashi, Y. Suginaka, S. Mori, M. Tatsumisago, *Electrochemistry* **2018**, *86*, 175.
- [27]. M. Mao, Z. Lin, Y. Tong, J. Yue, C. Zhao, J. Lu, Q. Zhang, L. Gu, L. Suo, Y. Hu, H. Li, X. Huang, L. Chen, *ACS Nano* **2020**, *14*, 1102.
- [28]. T. Yamada, S. Ito, R. Omoda, T. Watanabe, Y. Aihara, M. Agostini, U. Ulissi, J. Hassoun, B. Scrosatic, *J. Electrochem. Soc.* **2015**, *162*, A646.
- [29]. T. Matsuyama, A. Hayashi, C. J. Hart, L. F. Nazar, M. Tatsumisago, *J. Electrochem. Soc.* **2016**, *163*, A1730.
- [30]. A. L. Santhosha, N. Nazer, R. Koerver, S. Randau, F. H. Richter, D. A. Weber, J. Kulisch, T. Adermann, J. Janek, P. Adelhelm. *Adv. Energy Mater.* **2020**, *10*, 2002394.
- [31]. T. Matsuyama, M. Deguchi, K. Mitsuhashi, T. Oht, T. Mori, Y. Orikasa, Y. Uchimoto, Y. Kowada, A. Hayashi, M. Tatsumisago, *J. Power Sources* **2016**, *313*, 104.
- [32]. A. Sakuda, N. Taguchi, T. Takeuchi, K. Tatsumi, Z. Ogumi, *Solid State Ionics* **2014**, *262*, 143.
- [33]. M. Nagao, H. Kitaura, A. Hayashi, M. Tatsumisago, *J. Electrochem. Soc.* **2013**, *160*, A819.
- [34]. S. R. Narayanan, D. H. Shen, S. Surampudi, A. I. Attia, G. Halpert, *J. Electrochem. Soc.* **1993**, *140*, 1854.
- [35]. W. Xue, Z. Shi, L. Suo, C. Wang, Z. Wang, H. Wang, K. P. So, A. Maurano, D. Yu, Y. Chen, L. Qie, Z. Zhu, G. Xu, J. Kong, J. Li, *Nat. Energy* **2019**, *4*, 374.
- [36]. Y. Zhu, Y. Xu, Y. Liu, C. Luo, C. Wang, *Nanoscale* **2013**, *5*, 780.

- [37]. S. Wenzel, S. Randau, T. Leichtwei, D. A. Weber, J. Sann, W. G. Zeier, J. Janek, *Chem. Mater.* **2016**, *28*, 2400.
- [38]. J. Mao, K. Dai, M. Xuan, G. Shao, R. Qiao, W. Yang, V. S. Battaglia, G. Liu, *ACS Appl. Mater. Inter.* **2016**, *8*, 9116.
- [39]. D.-K. Kim et al., Effect of synthesis conditions on the properties of LiFePO<sub>4</sub> for secondary lithium batteries. *J. Power Sources* **159**, 237-240 (2006).
- [40]. S. R. Das, S. B. Majumder, R. S. Katiyar, *J. Power Sources* **2005**, *139*, 261.
- [41]. S. Y. Luchkin, K. Romanyuk, M. Ivanov, A. L. Kholkin, *J. Appl. Phys.* **2015** *118*, 072016.
- [42]. R. Fallahzadeh, N. Farhadian, *Solid State Ionics* **2015**, *280*, 10.
- [43]. Z. Zhang, Y. Shao, B. Lotsch, Y. Hu, H. Li, J. Janek, L. F. Nazar, C. Nan, J. Maier, M. Armand, L. Chen, *Energy & Environ. Sci.* **2018**, *11*, 1945.
- [44]. S. Cui, Y. Wei, T. Liu, W. Deng, Z. Hu, Y. Su, H. Li, M. Li, H. Guo, Y. Duan, W. Wang, M. Rao, J. Zheng, X. Wang, F. Pan, *Adv. Energy Mater.* **2016**, *6*, 1501309.
- [45]. W. Li, K. Wang, S. Cheng, K. Jiang, *Adv. Energy Mater.* **2019**, *9*, 1900993.
- [46]. X. Yao, N. Huang, F. Han, Q. Zhang, H. Wan, J. P. Mwizerwa, C. Wang, X. Xu, *Adv. Energy Mater.* **2017**, *7*, 1602923.
- [47]. A. Van der Ven, J. Bhattacharya, A. A. Belak, *Acc. Chem. Res.* **2013**, *46*, 1216.

[48]. H. Huo, J. Liang, N. Zhao, X. Li, X. Lin, Y. Zhao, K. Adair, R. Li, X. Guo, X. Sun, *ACS Energy Lett.*

**2020**, *5*, 2156.

[49]. P. G. Bruce, S. A. Freunberger, L. J. Hardwick, J. M. Tarascon, *Nat. Mater.* **2012**, *11*, 19.

[50]. H. Qu, J. Zhang, A. Du, B. Chen, J. Chai, N. Xue, L. Wang, L. Qiao, C. Wang, X. Zang, J. Yang, X.

Wang, G. Cui, *Adv. Sci.* **2018**, *5*, 1700503.

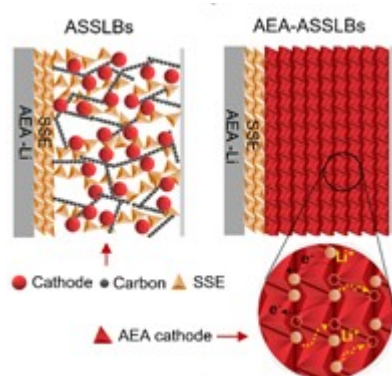
[51]. Y. Liu, P. He, H. Zhou, *Adv. Energy Mater.* **2018**, *8*, 1701602.

Author Manuscript

A new family of cathodes with superior ionic/electronic conductivities (AEA cathode) were demonstrated for all-solid-state Li metal battery. No carbon and electrolyte additives are needed in such AEA cathode so the space and mass of the electrode are fully utilized, and high mass/volume energy density are obtained.

Meiying Li, Tao Liu, Zhe Shi, Weijiang Xue, Yong-sheng Hu, Hong Li, Xuejie Huang, Ju Li, Liumin Suo, Liqun Chen

Dense All-Electrochem-Active Electrodes for All-Solid-State Lithium Batteries



ToC figure (size: 55 mm broad × 50 mm high))

This article is protected by copyright. All rights reserved.